



A preliminary study on the feasibility of industrialization for *n*-caproic acid recovery from food wastewater: From lab to pilot

Xiaoyu Zhu^{a,b,*}, Huanhuan Huang^{a,b,1}, Yong He^{a,b}, Xinyu Wang^{a,b,c}, Jia Jia^{a,b}, Xin Feng^{a,b}, Dong Li^{a,b}, Haixiang Li^c

^a CAS Key Laboratory of Environmental and Applied Microbiology, Environmental Microbiology Key Laboratory of Sichuan Province, Chengdu Institute of Biology, Chinese Academy of Sciences, Chengdu 610041, PR China

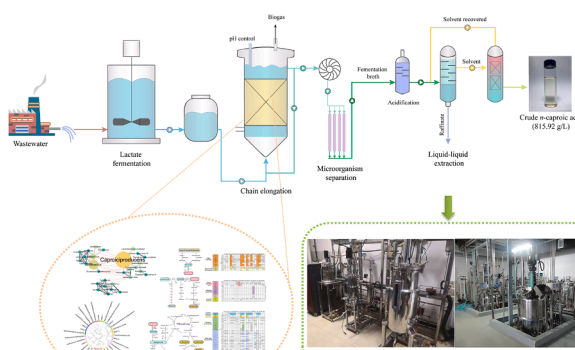
^b University of Chinese Academy of Sciences, Beijing 100864, PR China

^c Guangxi Key Laboratory of Environmental Pollution Control Theory and Technology, Guilin University of Technology, Guilin 541004, PR China

HIGHLIGHTS

- A pilot-scale process of *n*-caproate production from food wastewater was established.
- The highest production rate of *n*-caproate at lab-scale was 10.5 g/L/d.
- 14.5 g/L of *n*-caproate was achieved at pilot-scale without electron donor input.
- The concentration of *n*-caproic acid after extraction was 815.9 g/L.
- *Caproiciproducens* dominated the reactor microbiome.

GRAPHICAL ABSTRACT



ARTICLE INFO

Keywords:

Food wastewater
Lactate-driven chain elongation
n-Caproate
Caproiciproducens
Metagenomic analysis

ABSTRACT

Food wastewater is associated with greenhouse gas emission and has a significant water footprint. Here, the platform chemical *n*-caproate was recovered from liquor brewing wastewater at maximum and mean concentrations of 26.4 g/L and 17.0 ± 4.3 g/L, respectively, after 377 d operation. Laboratory-scale lactate-driven chain elongation (CE) process was implemented first. Taxonomic composition and metagenomic data analyses revealed that *Caproiciproducens* (e.g., Ruminococcaceae bacterium CPB6) and bacteria affiliated with Lachnospiraceae transformed lactate to *n*-caproate by reverse β-oxidation and/or fatty acid biosynthesis. The lactate-driven CE process was then scaled up from 2.5 L to 500 L and achieved a *n*-caproate production of 14.5 ± 0.6 g/L within 96 h. *n*-Caproic acid was extracted at a concentration and purity of 815.9 ± 8.3 g/L and 88.6 ± 8.9 %, respectively. The present study demonstrated a commercially viable strategy for resource recovery and carbon fixation from food waste streams.

Abbreviations: LBWW, Liquor brewing wastewater; CE, chain elongation; LF, lactate fermentation; AF, anaerobic filter; FAB, fatty acid biosynthesis; RBO, reverse β oxidation.

* Corresponding author at: CAS Key Laboratory of Environmental and Applied Microbiology, Environmental Microbiology Key Laboratory of Sichuan Province, Chengdu Institute of Biology, Chinese Academy of Sciences, Chengdu 610041, PR China.

E-mail address: zhuxy@cib.ac.cn (X. Zhu).

¹ Xiaoyu Zhu and Huanhuan Huang contribute equally to this paper.

<https://doi.org/10.1016/j.biortech.2022.128154>

Received 7 September 2022; Received in revised form 12 October 2022; Accepted 13 October 2022

Available online 18 October 2022

0960-8524/© 2022 Elsevier Ltd. All rights reserved.

1. Introduction

Over one-third of the food produced in the world is wasted through production, processing, distribution, retail, and consumption (Gustavsson et al., 2011), generating greenhouse gases, exacerbating climate change, and creating a negative water usage footprint (Jaglo et al., 2021). Neither the food system nor the environment is resilient if neither is sustainable. Recovery of chemicals from the food waste stream will promote waste disposal, recycling of renewable resources and reduction of CO₂ emissions (Angenent et al., 2016).

Chain elongation (CE) process potentially reduces food loss and waste by recovering *n*-caproic acid, a biofuel precursor and biochemical, from food waste streams (Candry et al., 2020; Crognale et al., 2021; Duber et al., 2018; Iglesias-Iglesias et al., 2021). *n*-Caproic acid has great potential as a platform chemical (Angenent et al., 2016; Chen et al., 2017). It can be processed into liquid biofuel alkane and alkenes (Harvey and Meylemans, 2014; Urban et al., 2017), fine chemicals such as fragrances, food additives, and pharmaceuticals (Liu et al., 2017; Wu et al., 2020), and bulk chemicals such as adipic acid used to fabricate nylon and bioplastics (Clomburg et al., 2015; Skoog et al., 2018). In CE process, functional microbiomes use carbon-carbon bonds (acetyl-CoA), energy (ATP) and reducing equivalents (e.g., NADH) from ethanol or lactate gradually elongate short-chain carboxylates (e.g., acetate and butyrate) into medium-chain carboxylates (e.g., *n*-caproate) (Barker et al., 1945; Zhu et al., 2017, 2015).

CE process is developing rapidly and two major branches have emerged: ethanol-driven and lactate-driven CE technologies. The ethanol-driven CE process is based on the principle of acidification of organic waste to obtain acetate/butyrate and the addition of ethanol to achieve the synthesis of *n*-caproate. The lactate-driven CE process is based on the principle of LF of organic waste to obtain lactate, which is followed by CE to synthesize *n*-caproate. For waste with low concentration of organic matters, such as waste activated sludge, the ethanol-driven CE process is more applicable. For organic waste with high concentration, such as acid whey and food waste, lactate-driven CE process is more suitable because acid whey and food waste can generate lactate itself, thus avoiding exogenous electron donor addition (Contreras-Dávila et al., 2020; Xu et al., 2017).

Both processes have been extensively studied, including different organic wastes conversion (waste activated sludge (Wang et al., 2021), swine manure, corn stalk silage (Zhang et al., 2022), cheese whey (Iglesias-Iglesias et al., 2021; Reddy et al., 2022), food waste (Contreras-Dávila et al., 2020; Crognale et al., 2021), switchgrass (Lin et al., 2019), etc.), microbiome community shaping and bioaugmentation (*Clostridium kluyveri* addition and granular sludge) (Lambrecht et al., 2019; Roghair et al., 2016; Zagrodnik et al., 2020), bioreactor types (UASB, membrane bioreactor, etc.) (Duber et al., 2018; Kim et al., 2022), optimization of process conditions (pH, hydraulic retention time HRT, organic loading rate OLR, etc.) (Kucek et al., 2016; Wu et al., 2020), variations of substrate ratios (Wang et al., 2018). These studies show that CE process is a promising process that can achieve the conversion of a vast majority of organic wastes to medium-chain carboxylates, e.g., caproate. If CE can be applied industrially, it will have a profound impact on the resource recovery of organic waste, no less than the classical anaerobic digestion for methane production (Aglar et al., 2014; Kim et al., 2022; Wu et al., 2021).

However, these studies also indicate that the CE process is still in its early stage and some problems are exposed: 1. Is the synthesis of *n*-caproate at low concentrations sufficient for industrialization? 2. The innovative extraction methods of *n*-caproate (e.g., hollow-fiber membrane extraction, electrodialysis/phase separation cell) (Xu et al., 2021a, 2021b) are technically difficult and not easily learned and used, yet there is no simple method reported; 3. CE process employed mixed microbiome to produce *n*-caproate from complex organic matters in an unsterilized environment, so is mixed microbiome still stable and capable of synthesizing *n*-caproate from real organic waste after

100–5000 times of scale-up? These three questions are crucial for the development of CE process, but none of the current studies positively answer them. And this research is aimed at giving a preliminary answer to these three questions.

Liquor brewing wastewater (LBWW) is a typical food waste produced during the food (liquor) process. In this study, LBWW was used to domesticate CE reactor microbiome for more than one year, and the efficacy of *n*-caproate production was tested at different HRTs and the key microorganisms and key metabolic pathways were investigated by high-throughput sequencing. Then, the fermentation system was expanded by 200 times to study the key conditions and feasibility of *n*-caproate production. Next, a simple, industrializable method was proposed for *n*-caproic acid extraction. Finally, the energy and chemical consumption during fermentation and extraction was accounted for and a preliminary economic benefit analysis was performed.

2. Materials and methods

2.1. Inoculum and the feedstock

The inoculum was taken from a long-term operating *n*-caproate-producing bioreactor cultured in a semi-continuous mode. The reactor microbiome was domesticated for more than three years, and was dominated by *Caproiciproducens* (Zhu et al., 2021). The feedstock was raw organic wastewater: LBWW, which was collected from liquor brewing factory in Sichuan province, PR China. The initial pH of LBWW was 3–4, which was adjusted to 5–6 by 5 M NaOH for LF. The LBWW was fermented naturally at 30 °C for 2 days. After LF, the total chemical oxygen demand (COD), soluble COD, total solid (TS), total suspended solid (TSS), protein, and soluble reducing sugar were estimated to be 227.4 ± 17.7 g/L, 196.2 ± 12.1 g/L, 147.2 ± 2.2 g/L, 0.3 ± 0.03 g/L, 9.7 ± 0.5 g/L, and 10.9 ± 0.4 g/L, respectively. Lactate, acetate, propionate, *n*-butyrate, *n*-valerate and ethanol were estimated to be 72.9 ± 3.6 g/L, 6.7 ± 0.3 g/L, 2.1 ± 0.1 g/L, 0.64 ± 0.1 g/L, 0.21 ± 0.07 g/L, and 29.3 ± 3.3 g/L, respectively. The wastewater was stored at 4 °C in the refrigerator for use.

2.2. Lab-scale experiment

The experiment was carried out in an anaerobic filter (AF) reactor with a total and a working volume of 5.0 and 2.5 L, respectively. The AF was made of acrylic acid and placed in a thermostatic room at a temperature of 30 ± 1 °C. A peristaltic pump (Longer, BT600-2 J, China) was used for recirculation from the lower to the upper chamber. The reactor was installed a pH monitor consisted of a pH transmitter (Hamilton, H100, Switzerland) and a pH electrode (Hamilton, 120 mm, Switzerland). The produced gases were collected in a gas-tight bag. LBWW was fed to the reactor by a peristaltic pump (Longer, BT100-2 J, China) at a continuous flow rate of 50 mL/min via an inlet in the recirculation tube.

The LBWW was mixed with the reactor microbiome inoculum (OD₆₀₀ 1.8) and tap water at the volume ratio of 1:1:3. The pH of the mixture was then adjusted to 6.0. The initial lactate loading was about 15 g/L. At the beginning, lactate was used for growth of the reactor microbiome and production of *n*-caproate. After 20 days of culture, raw LBWW was fed to the reactor without pH adjusting. The reactor was operated for a period of 24 h with a sequence of four steps: 1. external circulation (30 min); 2. drainage (5 min); 3. feeding (25 min); and 4. fermentation (23 h). The pH was manually adjusted to 6.0 once a day.

The long-term operation was divided into five stages: 1. setup (0–20 days); 2. phase I (21–58 days), *n*-caproate accumulation and domestication period at an HRT of 15 days; 3. phase II (59–120 days), domestication period for *n*-caproate production at an HRT of 10 days; 4. phase III (121–261 days), increasing *n*-caproate production at an HRT of 6 days; 5. phase IV (262–377 days), the stable *n*-caproate production at an HRT of 3 days.

2.3. Pilot-scale batch test

The pilot-scale batch test was conducted in a 550 L sealed fermentation reactor with a working volume of 500 L. The initial volume of fermentation was 200 L (LBWW 33 L and tap water 167 L). The initial pH was adjusted to 6.0 by 5 mol/L HCl or 5 mol/L NaOH. The reactor microbiome (OD₆₀₀ 2.0) was then inoculated into the reactor with a ratio of 6–20 % (v/v). When the synthesis of *n*-caproate was observed, LBWW was then continuously pumped from the liquid storage reactor into the anaerobic fermentation reactor at a speed of ~3L/h. Temperature was maintained at 28 ± 1 °C. Fig. 1 shows the process flow diagram for *n*-caproate production from LBWW.

2.4. Analysis of the microbial community

Samples (50 mL) were withdrawn from the reactors at different phases. All these samples were centrifuged at 12857 × g for 10 min, and then pellets were used for genomic DNA extractions. The information was detail in the previous research (Zhu et al., 2021).

2.5. Metagenomic DNA extraction, sequencing, and analysis

Two samples (50 mL) were withdrawn from the lab-scale reactors at the end of the experiment. The methods of DNA extraction, sequencing and analysis were the same as the previous research (Zhu et al., 2021).

2.6. Metagenomic assembly and binning

The clean reads and contigs were used for binning and refining genomes using MetaBAT2 (Parks et al., 2015) and Maxbin2. The genome bins were then checked for completeness and contamination using CheckM (Parks et al., 2018), and a total of 63 bins were selected after screening bins whose completeness were more than 80 % and contamination were <5 %. Genome taxonomy annotation was performed by TaxatorTK (Version:1.3.3) (Dröge et al., 2015) based on the NCBI_nt and NCBI_tax database. Genome functional annotation was performed by Prokka (version 1.14.6) based on the UniProtKB database (Seemann, 2014).

2.7. Phylogenetic analysis

Phylogeny of the bin genomes was assessed using 120 universal single-copy marker genes (bac120) with GTDB-tk v1.3.01 (Parks et al., 2018). 12 bins were used to construct a phylogenetic tree based on bac120 using Phylogeny.fr platform (Lemoine et al., 2019). The marker genes were aligned with MAFFT v7.407.1 (Katoh and Standley, 2013), construct phylogenetic tree based on the maximum-likelihood principle

with PhyML v3.3 (Guindon et al., 2010). Average nucleotide identities were calculated with JSpecies using the ANiB algorithm (Richter et al., 2016).

2.8. *n*-Caproic acid extraction

The extraction of *n*-caproic acid was operated with a sequence of five steps: centrifugation of fermentation broth for 5 mins at 1360 × g, membrane filtration, pH adjusted to 4.85, solvent (cyclohexane) extraction (1:1), and distillation. Fig. 1 shows the process flow diagram from fermentation to oily *n*-caproic acid extraction.

2.9. Calculations

The average production rate of each product (*n*-butyrate, *n*-valerate and *n*-caproate) was defined by its average concentration divided by the hydraulic retention time. The average selectivity of each product was based on the product-to-carboxylate production ratio in % mol C.

2.10. Chemical analysis

Liquid samples were collected daily, centrifuged for 5 min at 12857×g, diluted 20 times with distilled water and subsequently sterilized using a 0.22-μm filter. The methods for carboxylates (C1-C6), lactate and gases detection were presented in the previous research (Zhu et al., 2021).

2.11. Data availability

The raw sequence data (raw metagenomic sample data and raw 16S amplicon sample data) reported in this paper have been deposited in the National Center for Biotechnology Information (NCBI, <https://www.ncbi.nlm.nih.gov>) under accession number PRJNA851720 and PRJNA852677.

3. Results and discussion

3.1. Continuous laboratory-scale *n*-caproate production from LBWW

During long-term operation, *n*-caproate was produced from LBWW for 377 d. The reactor performance is depicted in Fig. 2 and Table 1. During the 20-d setup period, lactate was continuously fed into the bioreactor without draining to increase the *n*-caproate concentration. Meanwhile, the acetate, propionate, *n*-butyrate, and *n*-valerate concentrations slightly increased. The reactor was then operated in continuous mode with 15 d HRT. During Phase I (21–58 d), the reactor was in steady-state and the average concentration of *n*-caproate was 17.6 ± 2.0

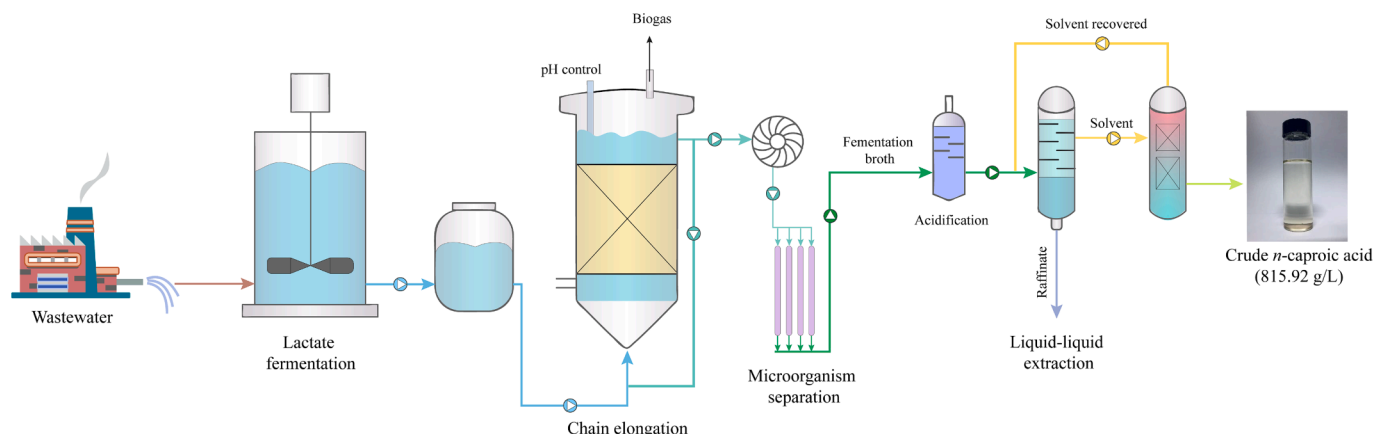


Fig. 1. Process flow diagram for *n*-caproic acid recovery from liquor brewing wastewater.

g/L (Fig. 2A and Table 1). The average production rate and selectivity of *n*-caproate were 1.7 ± 1.2 g/L and 64.5 ± 6.3 %, respectively (Fig. 2B and Table 1). The acetate and *n*-butyrate concentrations declined to ~ 1.2 g/L. The average propionate and *n*-valerate concentrations in the effluent were 2.0 ± 0.7 g/L and 4.1 ± 1.1 g/L, respectively (see supplementary materials). Over the next 61 d (Phase II), the HRT was shortened to 10 d. The *n*-caproate concentration first declined sharply from 19.6 g/L to 7.6 g/L. The acetate and *n*-butyrate concentrations significantly decreased to ~ 0.5 g/L. Then *n*-caproate production soon recovered and reached 15.3 g/L by day 84. The average *n*-caproate production in the bioreactor was 14.4 ± 1.4 g/L for 15 d. Over the next 20 d, the same dramatic swing in *n*-caproate production occurred. The average *n*-caproate concentration and selectivity in phase II fell to 12.1 ± 3.2 g/L and 54.0 ± 8.7 %, respectively. Compared to the long HRT of

phase I, however, the short HRT of Phase II significantly ($p = 0.036$) increased *n*-caproate production rate by 24.1 % and up to 2.1 ± 1.1 g/L.

During the following 140 d, HRT was further shortened to 6 d. The *n*-caproate concentration in the effluent gradually increased and stabilized at a mean level of 20.8 ± 1.7 g/L for 32 d. The maximum *n*-caproate concentration and production rate reached 26.4 g/L (day 261) and 8.7 g/L/d (day 180), respectively. The accumulation of ethanol was observed until day 191. This is because LBWW contains both ethanol and lactate, and the reactor microbiome cannot utilize ethanol (Zhu et al. 2015). After day 191, ethanol decreased significantly, and by day 200, ethanol concentration dropped below the detection line. At the same time, the proportion of methane in the biogas increased significantly, and the concentration of acetate also increased significantly (Fig. 2C). Ethanol oxidation and methane production from hydrogen

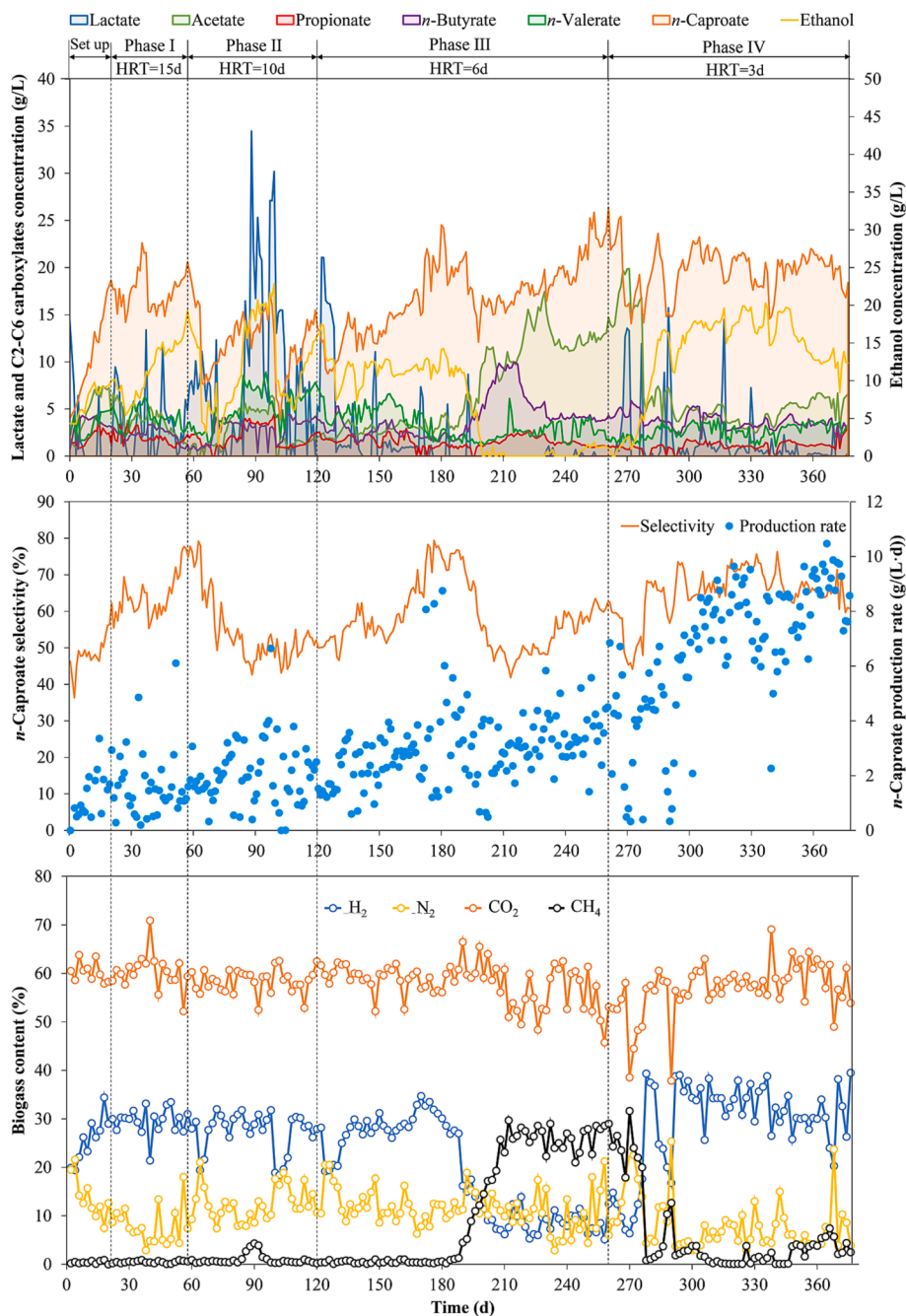


Fig. 2. Lab-scale reactor performance over the operating period of 377 days. Effluent C2-C6 carboxylates concentrations (A), *n*-caproate selectivity and production rate (B) and gases contents (C).

Table 1
Operating conditions and *n*-caproate production efficiency.

Phase	Time (d)	HRT (d)	Lactate loading rate (g/L/d)	<i>n</i> -Caproate					
				Concentration (g/L)		Production rate (g/L/d)		Selectivity (%)	
				Ave.	Max.	Ave.	Max.	Ave.	Max.
Phase I	21–58	15	4.9	17.6 ± 4.5	22.6	1.7 ± 1.1	6.1	64.5 ± 9.0	77.8
Phase II	59–120	10	7.3	12.1 ± 3.2	17.2	2.1 ± 1.1	6.6	54.0 ± 8.1	79.2
Phase III	121–261	6	12.1	17.0 ± 3.8	26.4	3.0 ± 1.4	8.7	58.2 ± 8.9	79.4
Phase IV	262–377	3	24.3	19.7 ± 2.3	25.4	6.6 ± 2.5	10.5	65.0 ± 6.7	76.3

occurred simultaneously. A Spearman's rank correlation analysis showed significant associations between ethanol oxidation and acetate ($\rho = -0.915$) and *n*-butyrate ($\rho = -0.701$) surge. Thus, ethanol was oxidized to acetate and part of the latter was elongated to *n*-butyrate. The *n*-butyrate accumulation lasted 25 d and gradually declined to its previous level thereafter. The *n*-caproate concentration and production rate were not declined by the decrease in hydrogen partial pressure ($p = 0.142$). The *n*-caproate production rate was 2.9 ± 1.6 g/L/d over 121–191 d, but in days 192–261, the rate increased to 3.2 ± 1.1 g/L/d. Ethanol oxidation might have had a positive effect on *n*-caproate production ($\rho = -0.378$) by significantly increasing the acetate concentration. During Phase III, the average *n*-caproate concentration, production rate, and selectivity were 17.0 ± 3.8 g/L, 3.0 ± 1.4 g/L/d, and 58.2 ± 9.0 g/L, respectively.

From day 262 onwards, HRT was further shortened to 3 d. The current maximum *n*-caproate concentration produced from real waste biomass without exogenous electron donor supplement was usually ~ 10 g/L (Duber et al., 2018). Over the next 115 d, the average and maximum *n*-caproate concentrations were increased to 19.7 ± 2.3 g/L and 25.4 g/L, respectively. The average and maximum *n*-caproate production rates were 6.6 ± 2.5 g/L/d and 10.5 g/L/d, respectively. The selectivity of *n*-caproate reverted to 65.0 ± 6.7 %. As HRT was shortened, the methane content in the biogas declined from 20.4 ± 8.9 % to 2.2 ± 1.9 % while the hydrogen content increased to 32.7 ± 4.5 % (Fig. 2C). Once again, ethanol accumulated in the reactor.

3.2. Dynamic changes and reactor microbiome ecological network

Sixteen samples were sequenced during the 377-d *n*-caproate production period. Structural biodiversity parameters including the Chao1, Shannon indices and the observed operational taxonomic units (OTUs) are presented in Table 2. Thirty-three bacterial genera with average relative abundance >0.1 % were identified in the samples and they comprised 97.4 % of the total microbial community. A phylum-level analysis revealed that Firmicutes predominated (mean 90.5 ± 10.6 %) in the community during the entire fermentation period. Actinobacteria had average relative abundance of 3.8 ± 3.3 %. Other minor phyla in the reactor microbiome were Proteobacteria (2.1 ± 7.2 %), Bacteroidetes (1.7 ± 6.4 %), and Euryarchaeota (1.3 ± 3.0 %) (see supplementary materials).

Fig. 3 shows that the *n*-caproate-producing bacterium *Caproiciproducens* (Ruminococcaceae) predominated. Its average relative abundance was 60.9 ± 24.2 %. The model species Ruminococcaceae strain CPB6 constituted 59.6 ± 18.6 % and 37.7 ± 20.1 % of *Caproiciproducens* and all taxa, respectively (Table 3). Lactate bacteria were the second most abundant and consisted mainly of *Lactobacillus* and *Enterococcus*. They comprised 19.8 ± 23.6 % of all taxa. The three dominant genera accounted for mean 80.7 ± 12.2 % of all taxa. Lachnospiraceae uncultured, Clostridiaceae Other, and *Clostridium* sensu stricto 12 had average relative abundances of 1.9 ± 1.5 %, 1.6 ± 2.2 %, and 1.3 ± 2.0 %, respectively. *Methanobacterium* represented only 1.3 ± 2.9 % of the entire community. *Methanobacterium* is a hydrogenotrophic methanogen and archaea and its abundance rose from 0.08 % (day 90) to 11.6 % by day 240 and fell to 0.5 % by day 270. The increase in relative abundance of *Methanobacterium* may be correlated with ethanol oxidation. First, an

Table 2
The microbial structural biodiversity.

Days	Chao1	Observed OTUs	Shannon
0	182.2	121	4.4
25	291.8	179	5.1
58	292.7	182	4.9
73	342.7	188	5.3
90	356.0	182	4.9
115	378.4	211	5.2
131	328.0	170	4.5
155	274.7	154	4.5
170	187.7	127	4.0
195	246.3	118	4.3
240	268.3	154	4.5
270	248.5	140	5.0
300	579.3	154	4.6
330	305.1	155	4.3
360	289.3	151	4.3
369	251.0	180	4.7

increase in ethanol concentration was observed throughout the first 120 days of fermentation. Meanwhile, the abundance of methanogens was only 0.02 ± 0.03 %. After the day 120, the relative abundance of methanogens began to increase intermittently, with an average value of 1.5 ± 0.2 %, while the ethanol concentration stopped increasing and remained at 10 g/L, indicating that some of the ethanol was oxidized. Between 191 and 270 days, the methanogens became more active, the average relative abundance increased to 4.2 ± 6.4 % with a maximum value of 11.6 % on day 240. During this period, the methane fraction in the gas increased rapidly, while hydrogen was consumed, and the ethanol concentration decreased until undetectable. The increase in *Methanobacterium* decreased the partial pressure of hydrogen, which accelerated ethanol oxidation. The shortening of HRT may have led to a significant decrease in the abundance of methanogens (mean value 0.5 ± 0.4 %), in parallel with the slowing down of ethanol oxidation and the accumulation of ethanol. The propionate producing *Cutibacterium* represented 0.2 ± 0.4 % of all taxa. When HRT was shortened to 3 d, the relative abundance of *Cutibacterium* decreased to a level below the detection limit.

Then, a microorganism co-occurrence network was constructed to explore the microbial community in detail. The topological structure showed that *Caproiciproducens* was the core of the community. *Caproiciproducens* was positively correlated with the nodes Lachnospiraceae uncultured (1.9 ± 1.5 %), Clostridiaceae 1 uncultured (0.6 ± 0.9 %), *Ruminiclostridium* 5 (0.2 ± 0.21 %), and Atopobiaceae Other (0.7 ± 0.9 %). These nodes positively connected with Ruminococcaceae uncultured (0.1 ± 0.3 %), Clostridiaceae Other (1.6 ± 2.2 %), *Clostridium* sensu stricto 13 (0.2 ± 0.5 %), *Clostridium* sensu stricto 15 (0.2 ± 0.4 %), *Haloimpatiens* (0.6 ± 1.7 %), and *Olsenella* (0.7 ± 0.7 %). Thus, *Caproiciproducens* and the ten foregoing nodes formed a subnetwork with relative abundance of 67.8 ± 26.9 % in the microbial community. All these nodes except *Clostridium* sensu stricto 13 showed positive relationships with *n*-caproate production ($0.1 < \rho < 0.7$, Fig. 3C). Hence, the subnetwork was named as the *n*-caproate association (CA) subnetwork. Lactate bacteria (*Lactobacillus* and *Enterococcus*) and seven other microbial co-occurrences formed another subnetwork with fully

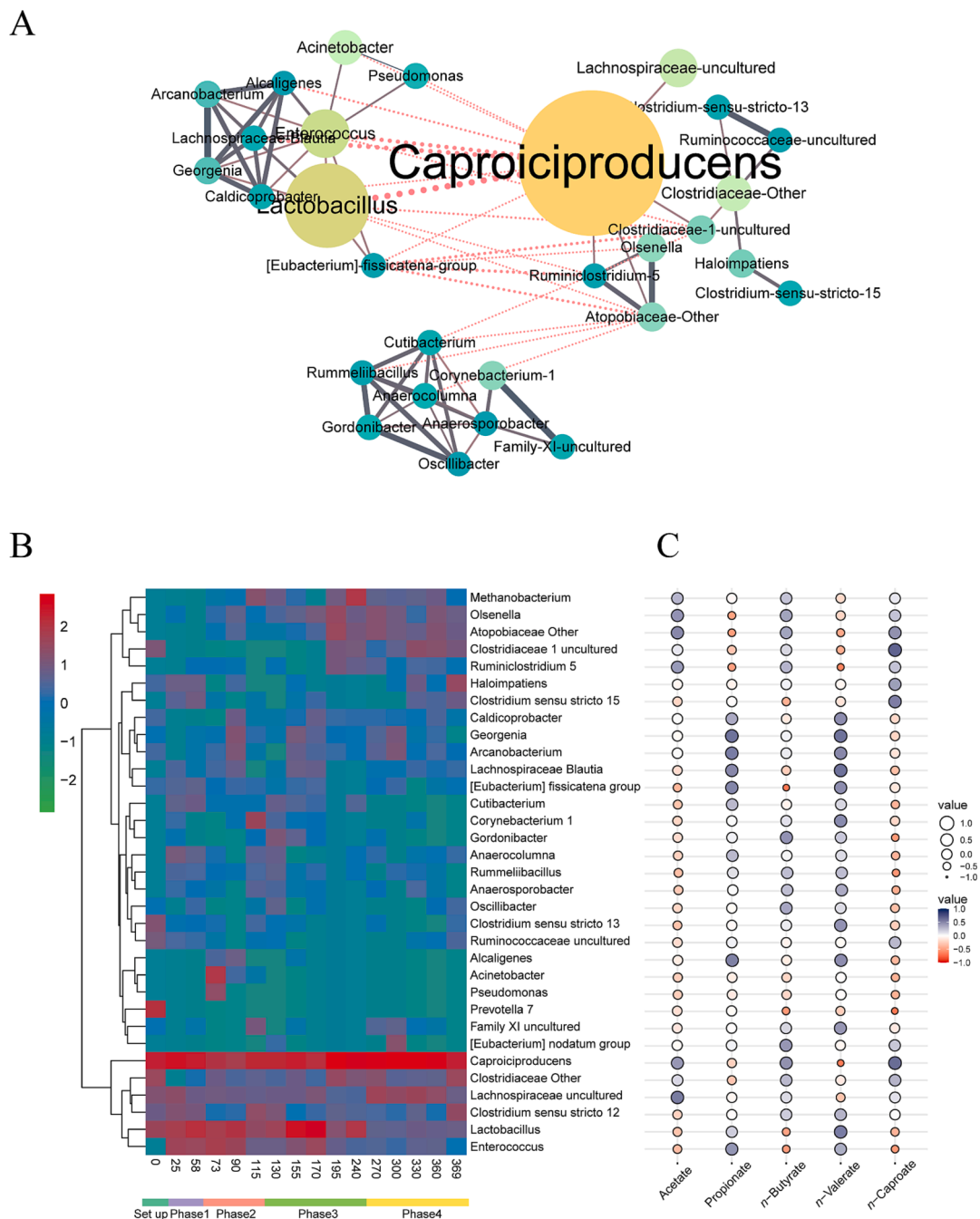


Fig. 3. Microbial co-occurrence network in the *n*-caproate-producing mixed microbiome at genus level (A) and variations in taxonomic community (B). Each node of network represents a genus whose size is proportional to the average relative abundance. Edges of network are also weighted by the strength of the correlation. Each edge represents a correlation between the two genera with a Pearson's correlation coefficient above 0.40. Solid and dashed lines represent a positive and negative correlation, respectively. Spearman's rank correlation between carboxylates production and relative genera (C). Blue and red colors indicate negative and positive correlations, respectively. Color saturation and size are proportional to the absolute value of the correlation coefficient. (For interpretation of the references to color in this figure legend, the reader is referred to the web version of this article.)

connected topology. *Caproiciproducens* was strongly negatively correlated with the *Lactobacillus* and *Enterococcus* in the second subnetwork. The third subnetwork consisted of eight nodes with total relative abundance of 2.4 ± 3.9 %. Representative bacteria included the propionate-producing *Cutibacterium* (0.2 ± 0.4 %) and possibly valerate-producing *Oscillibacter* (0.1 ± 0.3 %). The relative abundances of the nodes in the second and third subnetworks varied in the opposite direction of those nodes in the CA subnetwork (Fig. 3).

3.3. Prediction of the metabolic network profile by metagenome analysis

The predictive microbial metabolic network of the reactor microbiome was then investigated by analyzing the metagenome. 63 genome bins were successfully reconstructed based on the sequencing data (>80 % complete; <5 % contamination). Forty-three bins were categorized into 12 metagenome-assembled genomes (MAGs) based on their genetic homology (Table 4). The MAGs were then used in subsequent phylogenetic analysis (Fig. 4A). The predominant bacteria were assembled in the reactor microbiome, namely, Lactobacillaceae (MAG.2),

Table 3

Average relative abundance of *n*-caproate production-associated species during the 377-d *n*-caproate production period.

Species	relative abundance (%)
Ruminococcaceae_bacterium_CPB6	37.6 ± 20.1
Caproiciproducens_unclassified	12.8 ± 10.8
Caproiciproducens_uncultured_clostridium_sp.	6.5 ± 10.5
Caproiciproducens_uncultured_ruminococcus_sp.	3.6 ± 3.0
Lachnospiraceae_uncultured	1.0 ± 1.5
Haloimpatiens_uncultured_bacterium	0.8 ± 2.8
Caproiciproducens_uncultured_organism	0.6 ± 0.6
Clostridiaceae_1_uncultured_caloramator_sp.	0.5 ± 0.8
Clostridium_sensu_stricto_12_unclassified	0.5 ± 1.0
Haloimpatiens_unclassified	0.2 ± 0.4
Caproiciproducens_uncultured_clostridia_bacterium	0.2 ± 0.3
Olsenella_sp._Marseille-P3256	0.2 ± 0.3
Ruminiclostridium_5_unclassified	0.0015 ± 0.0057
Ruminococcaceae_uncultured_clostridium_sp.	0.0004 ± 0.0014
Clostridium_sensu_stricto_15_unclassified	0.0003 ± 0.0010
Caproiciproducens_uncultured_ruminococcaceae_bacterium	0.0002 ± 0.0007
Caproiciproducens_uncultured_bacterium	0.0 ± 0.0
Clostridium_sensu_stricto_12_unidentified	0.0 ± 0.0
Olsenella_scatoligenes	0.0 ± 0.0
Olsenella_sp._Marseille-P2300	0.0 ± 0.0
Olsenella_unclassified	0.0 ± 0.0
Olsenella_uncultured_bacterium	0.0 ± 0.0
Clostridiaceae_1_uncultured_clostridiales_bacterium	0.0 ± 0.0
Eubacterium]_nodatum_group_unclassified	0.0 ± 0.0
Eubacterium]_nodatum_group_unidentified	0.0 ± 0.0
Ruminococcaceae_CPB6_in_total_of_n-Caproate_production-associated_species	59.6 ± 18.6

Propionibacteriaceae (MAG.3), Lachnospiraceae (MAG. 1), Ruminococcaceae (MAG.6). The strains in MAG.6 had the highest homology to Ruminococcaceae bacterium CPB6 and UBA5408.

All functional genes in the metagenome were annotated against the KO database to elucidate the associated metabolic pathways including Embden-Meyerhof-Parnas pathway (EMP), amino acid metabolism, lactate and ethanol oxidation, CE, and propionate and methane production (see [supplementary materials](#)). Strains in the families Tissierellaceae, Clostridiaceae, Ruminococcaceae, Lactobacillaceae, Lachnospiraceae, Enterococcaceae, and Actinomycetaceae harbor genes encoding glycolytic enzymes that metabolize glucose to pyruvate. All predominant bacteria except Eggerthellaceae, Erysipelotrichaceae, Bacillaceae, and Propionibacteriaceae harbor genes encoding enzymes that convert amino acids into pyruvate. The latter is then transferred into organic acids or methane ([Fig. 4](#)).

CE-related cyclic pathways were identified: fatty acid biosynthesis (FAB) and reverse β oxidation (RBO). FAB and RBO might be performed by the Ruminococcaceae. Hence, members of this family contribute to

the conversion of lactate to *n*-caproate at the gene level. Lachnospiraceae also harbor all genes required for lactate and ethanol oxidation and FAB. Thus, the Lachnospiraceae may produce *n*-caproate. It was also found that the Corynebacteriaceae harbor all genes implicated in FAB. The model *n*-caproate-producing bacterium *Clostridium kluyveri* was also identified by metagenome sequencing and its relative abundance was 0.045 ± 0.0 %. Consequently, ethanol may be also involved in *n*-caproate production. However, the contribution of this bacterium to the synthesis of *n*-caproate is relatively small because of its very low abundance. The data in this study cannot directly show whether there is competition for ecological niches between *Clostridium kluyveri* and lactate utilizing *n*-caproate producing bacteria.

In the Wood-Werkman cycle, pyruvate is converted to propionate via a succinate intermediate. The Propionibacteriaceae harbor all the genes in the Wood-Werkman cycle. The Tissierellaceae, Eubacteriaceae, Peptococcaceae, Clostridiaceae, Lachnospiraceae, Oscillospiraceae, Enterococcaceae, and Actinomycetaceae harbor genes encoding lactate oxidation. The necessary genes in the acetotrophic methane production pathway were not found, but all genes in the hydrogenotrophic methane production pathway were detected in the Methanobacteriaceae.

3.4. Pilot-scale *n*-caproate production from LBWW

Chain Craft Co. carried out pilot-scale ethanol-driven CE but reported no relevant data ([Angenent et al., 2016](#)). To the best of our knowledge, the present study is the first to report on the efficiency of *n*-caproate recovery from real waste streams at pilot-scale. In the interest of cost recovery and reduction, neither the LBWW nor the fermentation reactor was sterilized. Five successful pilot-scale batch fermentations were performed, producing 2.5 t *n*-caproate fermentation broth.

The first batch exploration was failure. After a lag phase of 100 h, carboxylates began to be produced, and lactate was depleted. Thereafter, sodium lactate instead of real wastewater was supplied to the bioreactor. After 80 h, lactate was exhausted again, but the fermentation product was mainly acetate (6.3 g/L), with similar concentrations of *n*-butyrate (3.5 g/L), propionate (2.9 g/L), *n*-valerate (3.8 g/L) and *n*-caproate (3.5 g/L). The phenomenon suggests that at the initial stage of the fermentation, the caproate producing bacteria was failure to occupy an advantage in the microbial community.

In the second batch fermentation, the inoculation rate was increased from 6 % to 20 %. After 136.5 h of incubation, the *n*-caproate concentration increased rapidly from 2.0 g/L to 13.8 g/L. After that, the *n*-caproate concentration rose again and reached 14.9 g/L at 170.5 h. The acetate, *n*-butyrate, and *n*-valerate concentrations were 3.8 g/L, 3.0 g/L, and 2.2 g/L, respectively. No propionate was detected during fermentation. LBWW was used for feeding and observed ethanol accumulation. Another four batch fermentation trials were conducted. [Fig. 5](#) shows that the average *n*-caproate concentration and selectivity reached 14.5 ± 0.6 g/L and 59.7 ± 2.7 %, respectively. Apparently, *n*-caproate always predominated. The secondary product was *n*-valerate. Its average concentration was 3.9 ± 1.4 g/L and it constituted 14.7 ± 5.4 % of the total

Table 4

The detailed genomic characteristics of the bins.

Bin No.	Classification	Completeness (%)	Contamination (%)	GC (%)	N50 (bp)	Size (bp)
6	Lactobacillaceae	97.9	3.3	36.2	11,273	1,499,918
10	Propionibacteriaceae	99.3	0.00	69.0	47,960	3,384,832
35	Peptoniphilaceae	99.4	2.1	34.7	39,615	1,885,810
8	Erysipelotrichaceae	94.3	0.3	50.3	9969	2,214,715
11	Actinomycetaceae	80.4	2.3	56.9	6514	1,630,273
39	Lachnospiraceae	96.1	4.7	47.2	34,020	6,735,357
48	Bacillaceae	98.0	0.7	35.9	59,958	2,796,375
51	Corynebacteriaceae	98.2	1.0	67.0	182,097	2,988,605
70	Tissierellaceae	87.2	2.1	31.4	47,068	2,832,330
78	Ruminococcaceae	96.6	0.4	52.3	109,838	2,931,316
82	Oscillospiraceae	95.0	3.7	56.0	6308	2,807,413
83	Microbacteriaceae	98.8	0.0	71.5	227,340	1,963,424

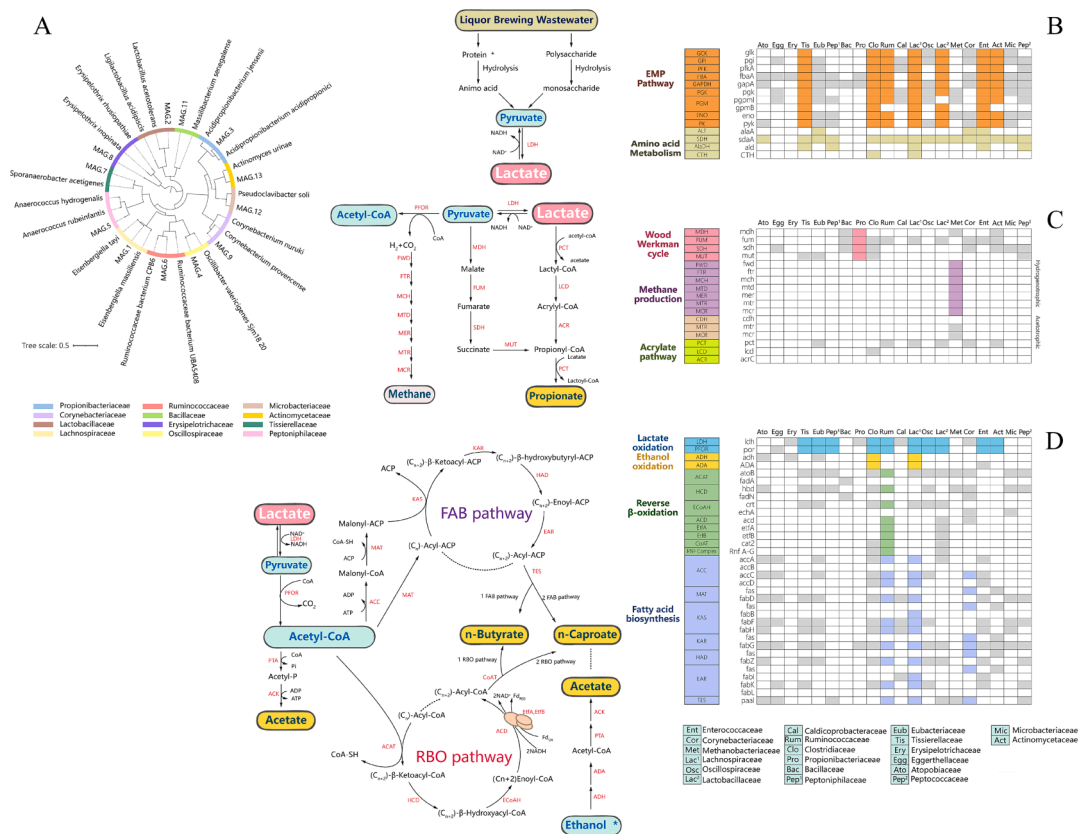


Fig. 4. Phylogenetic tree of the metagenome-assembled genomes (containing reconstructed genome 43 bins) obtained from reactor microbiome (A), and metabolic pathway profile with liquor brewing wastewater as feedstock and taxon function summarization and prediction based on 16S rRNA and metagenome sequences: (B) relative genes involved in the conversion of amino acid and glucose to pyruvate; (C) relative genes involved in the conversion of lactate to byproducts (methane and propionate); (D) relative genes involved in the conversion of lactate/ethanol to carboxylates (*n*-caproate, *n*-butyrate and acetate).

carboxylate product. The average acetate and *n*-butyrate concentrations in the effluent were 3.9 ± 0.2 g/L and 2.9 ± 0.4 g/L and they accounted for 10.4 ± 0.6 % and 10.5 ± 1.5 % of the total product, respectively. The

average concentration and selectivity of the propionate in the effluent were 1.5 ± 1.0 g/L and 4.6 ± 3.2 %, respectively.

Since the reactor microbiome we used in this study can only use

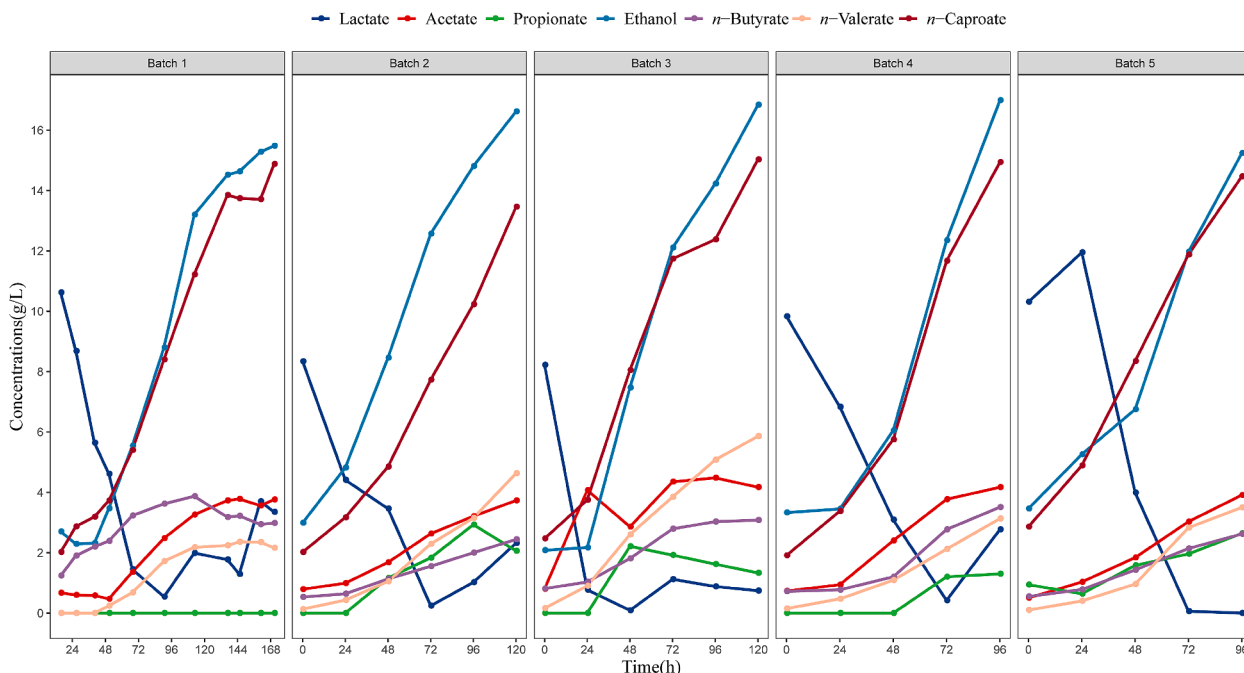


Fig. 5. *n*-Caproate production from liquor brewing wastewater at pilot scale.

lactate to produce *n*-caproate, the ethanol in LBWW was not used, resulting in a waste of resources. In future studies, we will try to combine the reactor microbiome with *Clostridium kluyveri*, which produces *n*-caproate from ethanol, to convert lactate and ethanol to *n*-caproate simultaneously.

3.5. Oily *n*-caproic acid extraction and cost analysis of energy and materials

The recovery of oily *n*-caproic acid from LBWW involved LF, CE, and liquid–liquid extraction requiring 48 h, 96–120 h, and < 24 h, respectively. Crude oily *n*-caproic acid was obtained from the fermentation broth. *n*-Butyric acid, *n*-valeric acid, and *n*-caproic acid were detected at concentrations of 16.7 ± 0.2 g/L, 34.2 ± 0.9 g/L, and 815.9 ± 8.3 g/L, respectively. Based on the density of *n*-caproic acid (921.2 g/L), the purity of the crude extract was 88.6 ± 8.9 % and the extraction rate was 85.7 ± 4.3 % (see [supplementary materials](#)). The website of Chain Craft Co. shows that they obtained *n*-caproic acid with a purity of 60 % (ChainCraft. Co. 2022). After the extraction of *n*-caproic acid by Xu et al, a mixture of medium-chain carboxylic acids, mainly octanoic acid (61 %), was obtained (Xu et al., 2021b). Here, the highest purity of *n*-caproic acid was reported.

An economic estimate was made on the basis of the laboratory- and pilot-scale trials (Table 5). The fermentation cost was determined mainly according to the chemical and energy consumption. The initial LBWW pH was ~4 and large amounts of hydroxide were required to increase it. Electricity was required to maintain the fermentation temperature at 28 °C. The solvent was the principal factor contributing to the extraction cost. In the laboratory-scale extraction experiment, the solvent loss was ~5 %. According to Chen et al., however, solvent loss can be reduced to 1 % in pilot-scale extraction systems (Chen et al., 2017). Even so, the solvent cost may represent 66.1 % of the total. Therefore, solvent loss has a significant impact on the total cost. A negative exponential correlation was determined between the *n*-caproate concentration and the extraction cost (see [supplementary materials](#)). When the concentration is increased from 3.7 g/L to 15 g/L, the cost is reduced by up to 66.5 %. If the price of crude *n*-caproic acid could increase to >~3,000 USD/t, the operation may become profitable only when the *n*-caproate product concentration is >7.5 g/L. If the price of *n*-caproic acid drops to ~2,000 USD/t, and wages and salaries, fixed asset investment, and raw material transportation costs are taken into account, the *n*-caproate concentration needed to be increased to ~15 g/L or the equipment efficiency needed to improve to reduce the loss of

Table 5
Costs required to produce 10 kg crude *n*-caproic acid.

Chemicals (\$)		
Fermentation ^a	Hydroxide ^c	2.00
Extraction ^b	Solvent ^d	10.7
	Hydrochloric acid ^e	0.06
Material loss (\$)		
	Membrane ^f	0.09
Energy ^g (\$)		
Fermentation ^a	Stirring	0.75
	Heating	2.50
Extraction ^b	Stirring	0.004
	Filtration	0.04
	Distillation	0.04
Total		16.19

^a Data based on pilot-scale experiment.

^b Data derived from laboratory-scale extraction experiment.

^c Price of hydroxide was 550.31 USD/t.

^d Cyclohexane recovery rate assumed to be 99% in pilot-scale system. Price of cyclohexane was 1,100 USD/t.

^e Price of hydrochloric acid was 20.44 USD/t.

^f Price of hollow fiber membrane (0.22 μm; 15 L/h) was 61.5 USD/column with lifespan = 3 y.

^g Price of electricity was 0.125 USD/kWh.

extractant. Hence, the concentration of the *n*-caproate and extraction process will determine the feasibility of CE industrialization.

In this study, the lactate in LBWW was utilized, but most of the ethanol was not. If lactate utilizing bacteria and ethanol utilizing bacteria can be mixed, it is possible to increase the concentration of *n*-caproate and thus reduce the extraction cost. However, the actual results are not certain, because competition between strains and feedback inhibition of *n*-caproate concentration may affect the *n*-caproate synthesis. However, it is worth to try the mixed method in the future.

3.6. Effect of lactate loading rate on *n*-caproate production

Lactate loading rate was significantly correlated with the *n*-caproate production rate ($\rho = 0.739$). After the rates at each stage were averaged, they were exponentially correlated with lactate loading rate ($R^2 = 0.9973$) (Fig. 6). This trend is consistent with that reported in a previous study (Kucek et al., 2016). However, the increase in lactate does not necessarily lead to propionate accumulation. This phenomenon may be related to the microbial community. Microflora with Ruminococcaceae as their core bacteria usually exhaust lactate, thereby avoiding propionate accumulation.

The increase in lactate loading rate is positively correlated with the relative abundance of *n*-caproate-producing bacteria ($\rho = 0.592$). When the bioreactor runs stably, increasing lactate loading enriches *n*-caproate-producing bacteria. Increases in the *n*-caproate production rate and the abundance of *n*-caproate-producing bacteria both increase the *n*-caproate concentration. Their associated correlation indices are 0.702 and 0.617, respectively.

However, it is relatively more difficult to increase *n*-caproate selectivity from 60 % to 80 % when real wastewater is used as the feedstock. The data showed that *n*-caproate selectivity was positively correlated with lactate loading rate and the abundance of *n*-caproate-producing bacteria. Nevertheless, their respective correlation indices were only 0.317 and 0.216. B. C. Kim et al. reported that when the operation mode was changed from semi-continuous to continuous, the propionate-producing bacteria were washed out of the system, *n*-caproate-producing bacteria dominated the community, and the *n*-caproate selectivity increased from 32.4 % to 81.3 % (Kim et al., 2022). Xu et al. stated that after the reactor was changed from single-phase to temperature-phased conversion and lactate loading was increased, the *n*-caproate selectivity increased from 23.3 % to 48.2 % (Xu et al., 2017). Duber et al. indicated that reducing the HRT increased the *n*-caproate selectivity from 55 % to 79 % (Duber et al., 2018). In this study, however, even though the relative abundance of *Cutibacterium* fell below the detection limit and the relative abundance of *n*-caproate-producing bacteria rose to 88.5 %, the *n*-caproate selectivity only fluctuated around 60.3 ± 9.0 %. This may be related to three reasons: 1). LBWW contains certain amounts of acetate, butyrate and propionate that may lower the ratio of *n*-caproate to total carboxylate in the effluent. 2). CE-associated bacteria may also use propionate to synthesize *n*-valerate. 3). *n*-Caproate-producing bacteria except strain CPB6 may also produce acetate and butyrate. For example, Ruminococcaceae strain CPB11 detected in the reactor microbiome produced nearly equal amounts of *n*-caproate and *n*-butyrate from lactate (Zhu et al., 2021).

3.7. *Caproiciproducens* was always the functional bacteria for *n*-caproate production

The most frequently reported functional genera in lactate-driven CE are *Caproiciproducens* (Kim et al., 2022; Wu et al., 2020; Zhang et al., 2022; Zhu et al., 2021, 2017, 2015) followed by *Megasphaera* (Jeon et al., 2017), *Pseudoramibacter* (Scarborough et al., 2020; Zhang et al., 2022), *Olsenella* (Duber et al., 2018; Iglesias-Iglesias et al., 2021), etc. Two species classified to *Caproiciproducens* have been more frequently reported, *Caproiciproducens galactitolivoran* (Kim et al., 2022, 2015) and Ruminococcaceae bacterium CPB6 (Wei et al., 2021; Zhu et al., 2021,

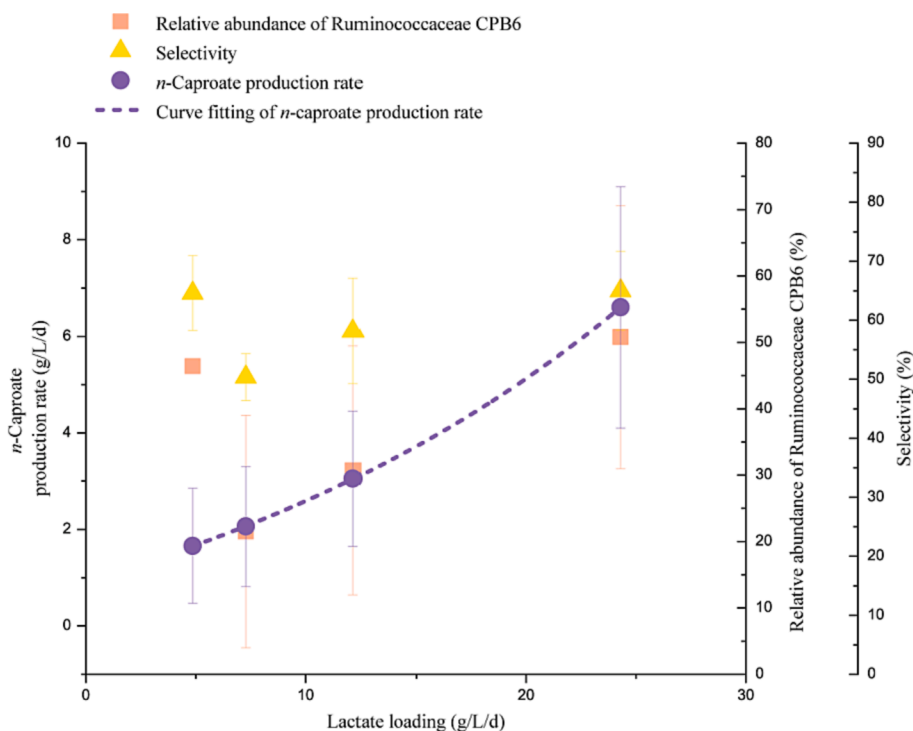


Fig. 6. Effect of lactate loading rate on *n*-caproate production, selectivity and relative abundance of Ruminococcaceae CPB6.

2017). The reactor microbiome dominated by the CPB6-related *Caproiciproducens* produced 33.7 g/L *n*-caproate using artificial wastewater (Zhu et al., 2021). The *Caproiciproducens* dominated reactor microbiome recovered 14.6 g/L *n*-caproate from restaurant food waste in a batch experiment (Wei et al., 2021). Here, the reactor microbiome produced 17.0 ± 4.3 g/L and 14.5 ± 0.6 g/L *n*-caproate (mean value) from real wastewater, LBWW, at the laboratory- and pilot scales, respectively. In addition, certain uncultured bacterial species were found that may also participate in *n*-caproate synthesis. Previously reported species included that Ruminococcaceae Other, Ruminococcaceae uncultured, *Ruminiclostridium* 5, Lachnospiraceae uncultured, and Clostridiaceae 1 uncultured (Zhu et al., 2021). Here, it was found that *Olsenella*, *Haloimpatiens*, *Clostridium sensu stricto* 15, and Atopobiaceae Other were also positively correlated with *n*-caproate synthesis. Nevertheless, no gene-level evidence for them was found. Real wastewater also decreased the relative abundance of *Methanobacterium* and increased the abundances of *Caproiciproducens* and *Lactobacillus* in the reactor microbiome community. The core flora comprised lactate- and *n*-caproate bacteria. The increase in lactate bacteria may be related to the carbohydrates such as sugars in LBWW.

3.8. The key factor and challenge for scale-up of lactate-driven reactor microbiome

CE utilizes the reactor microbiome to convert complex organic wastes into high-value, medium-chain carboxylates in an open (non-sterile) environment. The success of this process generally relies upon natural selection. The previous study showed that *n*-caproate-producing bacteria can naturally become the dominant bacteria when two environmental factors coexist, i.e., mild acid condition and lactate as substrate (Zhu et al., 2021). The present work confirmed that the reactor microbiome can maintain its function and efficiency at the pilot-scale trial level.

The experiment indicated the inoculation rate is vital to the process. Due to slow growth rate for anaerobic bacteria, the inoculation rate should be higher than 6%, and 10–20% was recommended. The low inoculation rate will result in the failure of the scale-up of reactor

microbiome.

pH is crucial for CE. Compared to the bio-system which was only 5 L, it was difficult to control the pH of a 500 L bio-system to 6.0 during the fermentation process for a large amount of hydrochloric/sulfuric acid consumption. Although the pH of the LF broth was low (4–5), it was not sufficient to offset the pH increase caused by the lactate-driven CE process. Therefore, the pH was higher than 6.5 after 4 days fermentation. pH control failure is not a limiting factor for batch fermentation, but for continuous flow fermentation, it may lead to the bio-system failure after long-term operation.

3.9. Effect of *n*-caproate concentration on industrialization

The *n*-caproate concentration affects the feasibility of CE. The extraction cost decreases with increasing *n*-caproate concentration. Xu et al. reported that the extraction (power consumption) cost of low *n*-caproate concentrations (<5.0 g/L) significantly increases when membrane electrolysis is used (Xu et al., 2021b). When the *n*-caproate concentration reaches 7.5 g/L, the total cost may be reduced to a level below the selling price. When fixed asset and labor costs are considered, however, it was suggested the *n*-caproate concentration should reach ~15 g/L (see supplementary materials).

Based on the literature and this study, the increase of *n*-caproate concentration was determined mainly by two factors, the functional microbiome and the lactate loading rate. A scale effect of *Caproiciproducens*-dominated bacteria was observed. Whereas the laboratory-scale reactor required 15–20 d to generate ~15 g/L *n*-caproate, the pilot-scale reactor needed only 4 d to reach the same target. Five successful pilot-scale batch experiments confirmed the stability of the reactor microbiome and the reproducibility of CE. Therefore, it is believed that the bio-systems can be scaled up 100-fold to a capacity of 50,000 L. The main obstacle may be the lactate loading rate. Without any external electron donor input (Han et al., 2019), a few of the previous reports can obtain ~15 g/L *n*-caproate from real waste streams.

3.10. Outlook

The Chinese liquor production reached to 6.6 million t in 2021, producing approximately 9.9–19.7 million t of LBWW. Our results indicated that nearly 15 g/L of *n*-caproate could be produced from LBWW, and extraction rate could reach to 85.7 %. If CE is implemented in all LBWW in China, 0.13–0.26 million t oily *n*-caproic acid could be recovered annually, thereby creating a value of 260–747 million USD/yr. Simultaneously, 0.15–0.3 million t CO₂ could be prevented from entering the atmosphere by being fixed in the form of *n*-caproic acid. Thus, the results of the present work will promote the application of a circular economic model wherein the carbon from food waste streams is recycled into a synthetic chemistry value chain and displaces the manufacture of products from fossil fuel or plant resources.

4. Conclusions

Lab-scale study showed the stability of the lactate-driven CE process in an open, non-sterilized condition with functional microorganisms consistently occupying the dominant ecological niche. The concentration of *n*-caproate is positively correlated with the lactate loading. Lactate-driven CE process can be quickly scaled up from lab-scale to pilot-scale. *n*-Caproic acid can be extracted from fermentation broth by a simple liquid–liquid extraction method. Industrialization of CE process may be economically feasible when the *n*-caproate concentration exceeds 7.5 g/L. This research confirms the industrial viability of CE process, but there are significant challenges ahead.

Author contributions

X.Y.Z. and H. X. L. designed the experiments; X.Y.Z., X.F., and J.J. performed the experiments; X.Y.Z., H.H.H., Y.H. and D. L. analyzed and interpreted the data; X.Y.Z. and H.H.H. drafted the manuscript. All the authors reviewed and critically revised the manuscript and approved the final version for publication.

Funding sources

This work was supported by the Natural Science Foundation of China (21777153, 52070089), Youth Innovation Promotion Association CAS, the Western Light Class A project CAS (2018XBZG_XBQNXZ_A_006), Chengdu Science and Technology Innovation Project (2022-YF05-00512-SN).

CRediT authorship contribution statement

Xiaoyu Zhu: Conceptualization, Investigation, Methodology, Formal analysis, Resources, Supervision, Writing – original draft, Writing – review & editing, Visualization, Data curation. **Huanhuan Huang:** Formal analysis, Software, Writing – original draft, Writing – review & editing, Visualization, Data curation. **Yong He:** Formal analysis, Investigation, Validation, Visualization. **Xinyu Wang:** Formal analysis, Investigation, Validation, Visualization. **Jia Jia:** Formal analysis, Investigation, Validation, Visualization. **Xin Feng:** Formal analysis, Investigation, Validation, Visualization. **Dong Li:** Formal analysis. **Haixiang Li:** Conceptualization.

Declaration of Competing Interest

The authors declare that they have no known competing financial interests or personal relationships that could have appeared to influence the work reported in this paper.

Data availability

Data will be made available on request.

Appendix A. Supplementary data

Supplementary data to this article can be found online at <https://doi.org/10.1016/j.biortech.2022.128154>.

References

- Agler, M.T., Spirito, C.M., Usack, J.G., Werner, J.J., Angenent, L.T., 2014. Development of a highly specific and productive process for *n*-caproic acid production: applying lessons from methanogenic microbiomes. *Water Sci. Technol.* 69, 62–68. <https://doi.org/10.2166/wst.2013.549>.
- Angenent, L.T., Richter, H., Buckel, W., Spirito, C.M., Steinbusch, K.J.J., Plugge, C.M., Strik, D.P.B.T.B., Grootsholten, T.I.M., Buisman, C.J.N., Hamelers, H.V.M., 2016. Chain elongation with reactor microbiomes: open-culture biotechnology to produce biochemicals. *Environ. Sci. Technol.* 50, 2796–2810. <https://doi.org/10.1021/acs.est.5b04847>.
- Barker, H.A., Kamen, M.D., Bornstein, B.T., 1945. The synthesis of butyric and caproic acids from ethanol and acetic acid by *Clostridium Kluyveri*. *Proc. Natl. Acad. Sci. U.S.A.* 31 (12), 373–381.
- Candry, P., Radić, L., Favere, J., Carvajal-Arroyo, J.M., Rabaey, K., Ganigué, R., 2020. Mildly acidic pH selects for chain elongation to caproic acid over alternative pathways during lactic acid fermentation. *Water Res.* 186, 116396. <https://doi.org/10.1016/j.watres.2020.116396>.
- ChainCraft. 2022, C-Craft Liquid <https://www.chaincraft.nl/project/c-craft-liquid/> (accessed 9.1.22).
- Chen, W.S., Strik, D.P.B.T.B., Buisman, C.J.N., Kroeze, C., 2017. Production of caproic acid from mixed organic waste: an environmental life cycle perspective. *Environ. Sci. Technol.* 51, 7159–7168. <https://doi.org/10.1021/acs.est.6b06220>.
- Clomburg, J.M., Blankschien, M.D., Vick, J.E., Chou, A., Kim, S., Gonzalez, R., 2015. Integrated engineering of β -oxidation reversal and ω -oxidation pathways for the synthesis of medium chain ω -functionalized carboxylic acids. *Metab. Eng.* 28, 202–212. <https://doi.org/10.1016/j.ymben.2015.01.007>.
- Contreras-Dávila, C.A., Carrión, V.J., Vonk, V.R., Buisman, C.N.J., Strik, D.P.B.T.B., 2020. Consecutive lactate formation and chain elongation to reduce exogenous chemicals input in repeated-batch food waste fermentation. *Water Res.* 169, 115215. <https://doi.org/10.1016/j.watres.2019.115215>.
- Crognale, S., Braguglia, C.M., Gallipoli, A., Gianico, A., Rossetti, S., Montecchio, D., 2021. Direct conversion of food waste extract into caproate: metagenomics assessment of chain elongation process. *Microorganisms* 9, 327. <https://doi.org/10.3390/microorganisms9020327>.
- Dröge, J., Gregor, I., McHardy, A.C., 2015. Taxator-tk: precise taxonomic assignment of metagenomes by fast approximation of evolutionary neighborhoods. *Bioinformatics* 31, 817–824. <https://doi.org/10.1093/bioinformatics/btu745>.
- Duber, A., Jaroszynski, L., Zagrodnik, R., Chwiałkowska, J., Juzwa, W., Ciesielski, S., Oleskiewicz-Popiel, P., 2018. Exploiting the real wastewater potential for resource recovery – *n*-caproate production from acid whey. *Green Chem.* 20, 3790–3803. <https://doi.org/10.1039/C8GC01759J>.
- Guindon, S., Dufayard, J.-F., Lefort, V., Anisimova, M., Hordijk, W., Gascuel, O., 2010. New algorithms and methods to estimate maximum-likelihood phylogenies: assessing the performance of PhyML 3.0. *Syst. Biol.* 59, 307–321. <https://doi.org/10.1093/sysbio/syq010>.
- Gustavsson, J., Cederberg, C., Sonesson, U., Otterdijk, R.M., 2011. Global food losses and food waste: extent, causes and prevention. Interpack 2011; Food and Agriculture Organization of the United Nations: Rome. Italy.
- Han, W., He, P., Shao, L., Lü, F., 2019. Road to full bioconversion of biowaste to biochemicals centering on chain elongation: a mini review. *J. Environ. Sci.* 86, 50–64. <https://doi.org/10.1016/j.jes.2019.05.018>.
- Harvey, B.G., Meylemans, H.A., 2014. 1-Hexene: a renewable C6 platform for full-performance jet and diesel fuels. *Green Chem.* 16, 770–776. <https://doi.org/10.1039/C3GC41554F>.
- Iglesias-Iglesias, R., Portela-Grandío, A., Treu, L., Campanaro, S., Kennes, C., Veiga, M.C., 2021. Co-digestion of cheese whey with sewage sludge for caproic acid production: role of microbiome and polyhydroxyalkanoates potential production. *Bioresour. Technol.* 337, 125388. <https://doi.org/10.1016/j.biortech.2021.125388>.
- Jaglo, K., Kenny, S., Stephenson, J., 2021. From Farm to Kitchen: The environmental impacts of U.S. food waste. U.S. Environmental Protection Agency Office of Research and Development 1–113.
- Jeon, B.S., Kim, S., Sang, B.-I., 2017. *Megasphaera hexanoica* sp. nov., a medium-chain carboxylic acid-producing bacterium isolated from a cow rumen. *Int. J. Syst. Evol. Microbiol.* 67, 2114–2120. <https://doi.org/10.1099/ijsem.0.001888>.
- Katoh, K., Standley, D.M., 2013. MAFFT multiple sequence alignment software version 7: improvements in performance and usability. *Mol. Biol. Evol.* 30, 772–780. <https://doi.org/10.1093/molbev/mst010>.
- Kim, H., Kang, S., Sang, B.-I., 2022b. Metabolic cascade of complex organic wastes to medium-chain carboxylic acids: a review on the state-of-the-art multi-omics analysis for anaerobic chain elongation pathways. *Bioresour. Technol.* 344, 126211. <https://doi.org/10.1016/j.biortech.2021.126211>.
- Kim, B.C., Seung Jeon, B., Kim, S., Kim, H., Um, Y., Sang, B.-I., 2015. *Caproiciproducens galactitolivorans* gen. nov., sp. nov., a bacterium capable of producing caproic acid from galactitol, isolated from a wastewater treatment plant. *Int. J. Syst. Evol. Microbiol.* 65, 4902–4908. <https://doi.org/10.1099/ijsem.0.000665>.
- Kim, B.C., Moon, C., Choi, Y., Nam, K., 2022a. Long-term stability of high-*n*-caproate specificity-ensuring anaerobic membrane bioreactors: controlling microbial

- competitions through feeding strategies. *ACS Sustainable Chem. Eng.* 10, 1595–1604. <https://doi.org/10.1021/acssuschemeng.1c07259>.
- Kucek, L.A., Nguyen, M., Angenent, L.T., 2016. Conversion of l-lactate into n-caproate by a continuously fed reactor microbiome. *Water Res.* 93, 163–171. <https://doi.org/10.1016/j.watres.2016.02.018>.
- Lambrecht, J., Cichocki, N., Schattner, F., Kleinstuber, S., Harms, H., Müller, S., Sträuber, H., 2019. Key sub-community dynamics of medium-chain carboxylate production. *Microb. Cell Fact.* 18, 92. <https://doi.org/10.1186/s12934-019-1143-8>.
- Lemoine, F., Correia, D., Lefort, V., Doppelt-Azeroual, O., Mareuil, F., Cohen-Boulakia, S., Gascuel, O., 2019. NGPhylogeny.fr: new generation phylogenetic services for non-specialists. *Nucleic Acids Res.* 47, 260–265. <https://doi.org/10.1093/nar/gkz303>.
- Lin, M., Dai, X., Weimer, P.J., 2019. Shifts in fermentation end products and bacterial community composition in long-term, sequentially transferred in vitro ruminal enrichment cultures fed switchgrass with and without ethanol as a co-substrate. *Bioresour. Technol.* 285, 121324. <https://doi.org/10.1016/j.biortech.2019.121324>.
- Liu, Y., He, P., Shao, L., Zhang, H., Lü, F., 2017. Significant enhancement by biochar of caproate production via chain elongation. *Water Res.* 119, 150–159. <https://doi.org/10.1016/j.watres.2017.04.050>.
- Parks, D.H., Imelfort, M., Skennerton, C.T., Hugenholtz, P., Tyson, G.W., 2015. CheckM: assessing the quality of microbial genomes recovered from isolates, single cells, and metagenomes. *Genome Res.* 25, 1043–1055. <https://doi.org/10.1101/gr.186072.114>.
- Parks, D.H., Chuvochina, M., Waite, D.W., Rinke, C., Skarshewski, A., Chaumeil, P.A., Hugenholtz, P., 2018. A standardized bacterial taxonomy based on genome phylogeny substantially revises the tree of life. *Nat. Biotechnol.* 36, 996–1004. <https://doi.org/10.1038/nbt.4229>.
- Reddy, M.V., Nandan Reddy, V.U., Chang, Y.-C., 2022. Integration of anaerobic digestion and chain elongation technologies for biogas and carboxylic acids production from cheese whey. *J. Cleaner Prod.* 364, 132670. <https://doi.org/10.1016/j.jclepro.2022.132670>.
- Richter, M., Rosselló-Móra, R., Oliver Glöckner, F., Peplies, J., 2016. JSpeciesWS: a web server for prokaryotic species circumscription based on pairwise genome comparison. *Bioinformatics* 32, 929–931. <https://doi.org/10.1093/bioinformatics/btv681>.
- Roghair, M., Strik, D.P.B.T.B., Steinbusch, K.J.J., Weusthuis, R.A., Bruins, M.E., Buisman, C.J.N., 2016. Granular sludge formation and characterization in a chain elongation process. *Process Biochem.* 51, 1594–1598. <https://doi.org/10.1016/j.procbio.2016.06.012>.
- Scarborough, M.J., Myers, K.S., Donohue, T.J., Noguera, D.R., Drake, H.L., 2020. Medium-Chain Fatty Acid Synthesis by “*Candidatus Weimeria bifida*” gen. nov., sp. nov., and “*Candidatus Pseudoramibacter fermentans*” sp. nov. *Appl Environ Microbiol* 86 (3).
- Seemann, T., 2014. Prokka: rapid prokaryotic genome annotation. *Bioinformatics* 30, 2068–2069. <https://doi.org/10.1093/bioinformatics/btu153>.
- Skoog, E., Shin, J.H., Saez-Jimenez, V., Mapelli, V., Olsson, L., 2018. Biobased adipic acid – the challenge of developing the production host. *Biotechnol. Adv.* 36, 2248–2263. <https://doi.org/10.1016/j.biotechadv.2018.10.012>.
- Urban, C., Xu, J., Sträuber, H., dos Santos Dantas, T.R., Mühlenberg, J., Härtig, C., Angenent, L.T., Harnisch, F., 2017. Production of drop-in fuels from biomass at high selectivity by combined microbial and electrochemical conversion. *Energy Environ. Sci.* 10 (10), 2231–2244.
- Wang, H., Li, X., Wang, Y., Tao, Y., Lu, S., Zhu, X., Li, D., 2018. Improvement of n-caproic acid production with Ruminococcaceae bacterium CPB6: selection of electron acceptors and carbon sources and optimization of the culture medium. *Microb. Cell Fact.* 17, 99. <https://doi.org/10.1186/s12934-018-0946-3>.
- Wang, Y., Wei, W., Wu, W., Sun, J., Xu, Q., Wang, D., Song, L., Ni, B.-J., 2021. Improving medium-chain fatty acid production from anaerobic fermentation of waste activated sludge using free ammonia. *ACS Environ. Sci. Technol. Eng.* 1, 478–489. <https://doi.org/10.1021/acsestengg.0c00179>.
- Wei, Y., Ren, B., Zheng, S.R., Feng, X., He, Y., Zhu, X.Y., Zhou, L.X., Li, D., 2021. Effect of high concentration of ammonium on production of n-caproate: recovery of a high-value biochemical from food waste via lactate-driven chain elongation. *Waste Manage.* 128, 25–35. <https://doi.org/10.1016/j.wasman.2021.04.015>.
- Wu, Q., Jiang, Y., Chen, Y., Liu, M., Bao, X., Guo, W., 2021. Opportunities and challenges in microbial medium chain fatty acids production from waste biomass. *Bioresour. Technol.* 340, 125633. <https://doi.org/10.1016/j.biortech.2021.125633>.
- Wu, S., Sun, J., Chen, X., Wei, W., Song, L., Dai, X., Ni, B.J., 2020. Unveiling the mechanisms of medium-chain fatty acid production from waste activated sludge alkaline fermentation liquor through physiological, thermodynamic and metagenomic investigations. *Water Res.* 169, 115218. <https://doi.org/10.1016/j.watres.2019.115218>.
- Xu, J., Hao, J., Guzman, J.J.L., Spirito, C.M., Harroff, L.A., Angenent, L.T., 2017. Temperature-phased conversion of acid whey waste into medium-chain carboxylic acids via lactic acid: no external e-donor. *Joule* 3, 885–888. <https://doi.org/10.1016/j.joule.2019.02.009>.
- Xu, J., Bian, B., Angenent, L.T., Saikaly, P.E., 2021a. Long-term continuous extraction of medium-chain carboxylates by pertraction with submerged hollow-fiber membranes. *Front. Bioeng. Biotechnol.* 9, 726946. <https://doi.org/10.3389/fbioe.2021.726946>.
- Xu, J., Guzman, J.J.L., Angenent, L.T., 2021b. Direct medium-chain carboxylic-acid oil separation from a bioreactor by an electrodialysis/phase separation cell. *Environ. Sci. Technol.* 55, 634–644. <https://doi.org/10.1021/acs.est.0c04939>.
- Zagrodnik, R., Duber, A., Lęzyk, M., Oleskiewicz-Popiel, P., 2020. Enrichment versus bioaugmentation—microbiological production of caproate from mixed carbon sources by mixed bacterial culture and *Clostridium kluyveri*. *Environ. Sci. Technol.* 54, 5864–5873. <https://doi.org/10.1021/acs.est.9b07651>.
- Zhang, W., Wang, S., Yin, F., Cao, Q., Lian, T., Zhang, H., Zhu, Z., Dong, H., 2022. Medium-chain carboxylates production from co-fermentation of swine manure and corn stalk silage via lactic acid: without external electron donors. *Chem. Eng. J.* 439, 135751. <https://doi.org/10.1016/j.cej.2022.135751>.
- Zhu, X., Tao, Y., Liang, C., Li, X., Wei, N., Zhang, W., Zhou, Y., Yang, Y., Bo, T., 2015. The synthesis of n-caproate from lactate: a new efficient process for medium-chain carboxylates production. *Sci. Rep.* 5, 14360. <https://doi.org/10.1038/srep14360>.
- Zhu, X., Zhou, Y., Wang, Y., Wu, T., Li, X., Li, D., Tao, Y., 2017. Production of high-concentration n-caproic acid from lactate through fermentation using a newly isolated Ruminococcaceae bacterium CPB6. *Biotechnol. Biofuels* 10, 102. <https://doi.org/10.1186/s13068-017-0788-y>.
- Zhu, X., Feng, X., Liang, C., Li, J., Jia, J., Feng, L., Tao, Y., Chen, Y., Nojiri, H., 2021. Microbial ecological mechanism for long-term production of high concentrations of n-caproate via lactate-driven chain elongation. *Appl. Environ. Microbiol.* 87 (11) <https://doi.org/10.1128/AEM.03075-20>.